The magnetic structure and phase transitions of holmium-yttrium alloys

1994 J. Phys.: Condens. Matter 6 2985

(http://iopscience.iop.org/0953-8984/6/16/004)

J. Phys.: Condens. Matter 6 (1994) 2985–2998. Printed in the UK

The magnetic structure and phase transitions of holmium–yttrium alloys

R A Cowley†, R C C Ward†, M R Wells†, M Matsuda‡§ and B Sternlieb‡

† Oxford Physics, Clarendon Laboratory, Parks Road, Oxford OX1 3PU, UK

‡ Physics Department, Brookhaven National Laboratory, Upton, NY 11973, USA

Received 28 January 1994

Abstract. Films of holmium–yttrium alloys were grown by molecular beam epitaxy (MBE), and found to have a mosaic spread of about 0.2°, a concentration uniformity of better than 0.5% and a concentration accuracy of better than 2%. Neutron scattering techniques at the Brookhaven HFBR were used to study the magnetic structures and phase transitions of four samples Ho_xY_{1-x} with $x = 1.0, 0.9, 0.7$ and 0.5 in zero field, and one sample with $x = 0.7$ as a function of applied magnetic field. In zero field the structures are all helical structures with the moments in the basal planes and the wavevectors of the helix along the hexagonal c-axis. At T_N, the wavevectors are $0.282c^*$, and decrease on cooling, until at low temperatures the structures become commensurate with wavevectors of $\frac{1}{5}c^*(x = 1)$, $\frac{2}{9}c^*(x = 0.9)$, $\frac{1}{4}c^*(x = 0.7)$ and $\frac{4}{15}c^*(x = 0.5)$. The critical exponent β was measured for each of the films and is consistent for all of the materials with $\beta = 0.50 \pm 0.05$. There is some rounding at T_N which may be due to the second and long length scale that has been found in pure holmium. When a magnetic field between 0 and 6 T is applied in the basal plane, the phase diagram for $x = 0.7$ has six phases. On cooling in a low field the sequence is paramagnetic, incommensurate helix, $q = \frac{1}{4}$ helix, while for fields above 4 T, the sequence is paramagnetic, incommensurate fan, $q = \frac{1}{4}$ fan. On increasing the field the helical phase goes directly to the fan phase, but on decreasing the field from the $q = \frac{1}{4}$ fan phase, the system shows a $q = \frac{1}{4}$ helifan phase between the fan and helical phases.

1. Introduction

Random magnetic systems are of interest both for their magnetic structures and the critical properties associated with the phase transitions. Many of the studies are, however, made difficult by the problem of ensuring that the random material has a uniform composition and that unusual properties do not result from macroscopic inhomogeneities. In this paper we have used an unusual way of growing rare-earth alloys by using the MBE facility at the University of Oxford to grow single-crystal epitaxial films of holmium/yttrium alloys as described in section 2, and these were then found to be of very high crystallographic quality and of macroscopically uniform composition. The details of the x-ray and neutron scattering characterization are given in section 2.

The alloys grown are Ho_xY_{1-x} with nominal values of x of 1.0, 0.9, 0.7 and 0.5. These alloys were first studied by Child *et al* (1965) who used neutron powder diffraction techniques to study this alloy system, and found that the alloys were magnetically ordered below T_c into a helical phase. Our measurements confirm this result and in section 3 we present detailed measurements of the magnetic structure as a function of temperature

§ Permanent address: Institute of Physical and Chemical Research, Hirosawa 2-1, Wasko-shi, Saitama 351-01, Japan.

0953-8984/94/162985+14$19.50

and field. One reason for our choice of the Ho_xY_{1-x} system is that the phase transition in bulk holmium has been the subject of controversy. Theoretically Bak and Mukamel (1976) calculated the critical exponents as $\beta = 0.39$ and $\alpha = -0.17$ while Kawamura (1988) obtained $\beta = 0.25$ and $\alpha = 0.4$, and Barak and Walker (1982) obtained a first-order transition. Experimental measurements of β (Eckert and Shirane 1976, Gaulin *et al* 1988) gave $\beta = 0.39 \pm 0.04$ while α was measured as 0.27 by Jayasuraya *et al* (1985) and between 0.1 and 0.2 by Wang *et al* (1991). Most recently Thurston *et al* (1993) showed that the critical phenomena in bulk holmium had two length scales and suggested that the detailed behaviour might depend on the surface effects. We have therefore examined the behaviour of the order parameter because the surface of our holmium film was capped with yttrium, and so was not oxidized unlike the surface of a bulk holmium crystal. We have also studied the behaviour of the alloy materials because if the exponent α is positive for holmium, the behaviour in the random alloy is predicted to be different from that of the pure materials (Harris 1974), and since some of the theories predict that α is large and positive, this difference in behaviour might be significant. The results of the studies of the critical phenomena are presented in section 4. We have also studied one of the alloys, with $x = 0.7$ when a magnetic field is applied in the basal plane. The initial reason for this was to study the effect of the field on the helical structure because it was suspected that the application of a field might destroy the long-range helical order. The effect of a magnetic field on the helical structure in a random material might be expected to pin the phase of the structure in regions of high concentration of magnetic ions. This is equivalent to applying a random field conjugate to the continuous order parameter, which is expected to destroy the long-range order. Long-range order was not, however, destroyed. Nevertheless, the resulting phase diagram showed a variety of phases, including a helifan phase, and marked metastability as described in section 5. The results are summarized in the final section.

2. The random alloy samples

2.1. Sample growth

The series of holmium–yttrium alloy samples (Ho_xY_{1-x}) were grown by MBE using a Balzers UMS630 facility. The growth techniques employed follow the procedures first developed by Kwo *et al* (1985) for rare-earth metal superlattices. The rare-earth metals grow epitaxially onto a niobium metal layer deposited on a sapphire (Al_2O_3) substrate; the Nb acts as a chemical buffer to prevent reaction between the rare earth and the sapphire. The BCC Nb and the HCP rare-earth metals grow with their respective close-packed atomic planes parallel to the substrate plane. The epitaxial relationships are {110} Al_2O_3 || {110} Nb|| {001} Y, Ho. An Y seed layer is grown on the Nb buffer to a thickness (about 1000 Å) above the critical thickness at which the Y lattice relaxes back to its bulk value. The Ho/Y alloy is then grown on this seed layer to the desired thickness, in this case 5000 Å. Finally a capping layer of Y of thickness 300 Å is added to inhibit oxidation of the alloy when the sample is exposed to air.

The temperature at which the bulk alloy layer should be grown is an important issue. For a superlattice sample with discrete layers of different material, a growth temperature is selected that minimizes interdiffusion at the interface whilst at the same time providing sufficient surface mobility to promote a layer-by-layer growth mode; for example, in the MBE growth of Ho/Y superlattices we have used a temperature of between 300 and 400 °C (Jehan *et al* 1993). In the case of a single alloy layer, interdiffusion is advantageous for growing a homogeneous Ho/Y phase. In the series of Ho/Y alloys reported on here a

growth temperature of 550 °C was used, which the neutron diffraction experiments verify as producing a highly uniform alloy. The higher growth temperature also promotes good crystallinity of the layer.

The normal growth rate for a single element of our superlattice samples is about 0.5 Å s^{-1} and this rate was maintained for the combined evaporation of the two elements Ho and Y. Holmium was evaporated from a standard Knudsen effusion cell (with a BN crucible). Yttrium requires an electron-beam source, in our case controlled via a quadrupole flux monitor. The deposition rates of both sources were calibrated using an *in situ* quartz crystal monitor. Therefore the flux setting for the electron-beam evaporator and the temperature of the effusion cell could be set to provide the designated percentage fraction x of the alloy under the normal conditions of controlled deposition of 0.5 Å s^{-1}.

Clearly there are limitations to these settings, particularly for the electron-beam evaporation, where experiment indicates that a constant long-term rate is not always achieved despite the quadrupole control of the power source. This is because, for materials like rare earths, at relatively low evaporation rates, only a fraction of the total material in the hearth is at the required evaporation temperature, mainly because of the low thermal conductivity of the material. This results in 'pitting' of the rare-earth material and brings about a change in the profile of the evaporating flux, for which the quadrupole monitor control is unable to compensate. Despite these difficulties the resulting alloys are found to be excellent in their quality—homogeneity and designated composition being very close to the designated values.

2.2. *Sample characterization*

The samples were examined at room temperature by x-ray diffraction techniques using a high-resolution triple-crystal diffractometer mounted on a STOE rotating-anode x-ray generator in Oxford. Scans were performed to determine the profile of the (002) Bragg reflections from the alloys. The mosaic spread of the alloys and the c-axis lattice parameters are listed in table 1. The mosaic spread is much larger than that of the Al_2O_3 substrate, $< 0.003°$, or the Nb layer, $< 0.003°$, and presumably results from the lack of perfect epitaxy of the rare earth onto the niobium. The c-axis lattice parameters were determined by comparing the peak positions with those of the sapphire substrate. The holmium film ($x = 1$) lattice parameter is smaller than the bulk lattice parameter, 5.6178 Å, presumably because the epitaxial growth on the yttrium substrate expands the a-axis lattice parameter leading to a contraction along the c-axis. The concentration of the films was then deduced by assuming that the lattice parameter is linearly dependent on the concentration difference between the measured Y c-axis parameter, 5.7306 Å, and the holmium film lattice parameter. The results are listed in table 1, and agree with the nominal concentration to 2%. Scans through the (002) Bragg reflection to measure the uncertainty in the lattice parameter showed a broadening, FWHM, of about 0.030° for each of the samples. The resolution of the instrument is about 0.008°, and the broadening due to the finite thickness of the alloy is 0.016° showing that there is a further spread in the lattice parameter of about 0.0015 Å, which may arise either from concentration fluctuations of about 1.4% or from a homogeneous relaxation of the lattice parameter throughout the alloy layer.

The neutron scattering measurements at the Brookhaven HFBR, described in the following sections, enabled measurements to be made of the magnetic ordering temperatures, T_c, as listed in table 1. As found by Child *et al* (1965), T_c decreases less rapidly than x on introducing yttrium into the sample. Child *et al* suggest that $T_c \sim x^{0.67}$, whereas our data yield $T_c \sim x^{0.56\pm0.05}$. Fits to the order parameter were also made, section 4, in which a spread in T_c was assumed. The spreads obtained were typically 0.6 K ($x = 1$), 0.43 K

($x = 0.9$), 1.0 K ($x = 0.7$) and 0.6 K ($x = 0.5$). We conclude that the increase in the width in the alloys due to concentration fluctuations is less than 0.7 K suggesting that these fluctuations are of less than 0.5%. We therefore conclude that the LAMBE facility is capable of producing single-crystal random-alloy samples with a mosaic spread of 0.2°, and with the concentration accurate to 2% and concentration fluctuations of less than 0.5%. These are specifications that it is very hard to meet with conventional bulk crystal growth techniques.

2.3. Neutron scattering experiment

The neutron scattering experiments were performed on the H9 spectrometer at the Brookhaven High Flux Beam Reactor. The H9 spectrometer is situated on the cold source with a double-graphite (002) monochromator with collimation between the reactor and sample of 60′–40′–60′, and then a graphite (002) analyser with collimation of 40′ between it and the sample and similarly between the analyser and the detector. The spectrometer was largely operated so as to record the elastic scattering, and the incident neutron energy was fixed at 5 meV. Because the sample was very thin it was found that the count rate depended on the relative orientation of the sample and the collimator blades of the analyser and detector. The central blades of both the monochromator–sample and sample–analyser collimators were therefore removed when the resolution became a smooth regular function. The resulting wavevector resolution, FWHM, for elastic scattering at the (002) Bragg peak was 0.010 Å^{-1} along c^*, 0.016 Å^{-1} in the scattering plane and perpendicular to c^*, and 0.08 Å^{-1} perpendicular to the scattering plane. Some of the measurements were performed for wavevector transfers close to the spiral wavevector $0.27c^*$ where the resolution was 0.025 Å^{-1} along c^*, and 0.003 Å^{-1} perpendicular to c^*.

The samples were mounted in a closed-cycle cryostat with the a^*, c^* plane horizontal, so that the temperature could be controlled to ±0.05 K. For the measurements in a magnetic field, the $x = 0.7$ sample was mounted in a variable-temperature cryostat inside a superconducting magnet with the field aligned perpendicular to the scattering plane. The magnetic field was varied between 0 and 6 T with an accuracy of 0.05 T and the temperature controlled to 0.2 K.

3. The magnetic structure of Ho/Y alloys

On cooling the magnetic alloys, the magnetic structure was measured by scanning the wavevector transfer along the $(00L)$ direction. The results showed that long-range helical magnetic order is established, and from the width of the diffraction peaks along both $(00L)$ and in a perpendicular direction, no evidence was observed for any break-up of the long-range helical order, either parallel or perpendicular to the growth direction. The position of the peaks for the four samples are shown in figure 1 as a function of temperature, and the wavevector at the onset of long-range order is $0.282 \pm 0.002c^*$ for all the samples, corresponding to a turn angle from layer to layer of 51.0 ± 0.2°. On cooling the sample, the wavevector decreases with the decrease being largest for the pure Ho layer. At low temperatures, below 30 K, the wavevector becomes independent of temperature, and additional weak peaks are observed corresponding to fifth and seventh harmonics of the primary wavevector. The positions of these peaks give accurate values for the low-temperature wavevectors of the helical structure as 0.271 ± 0.002 for $x = 0.5$, 0.251 ± 0.002 for $x = 0.7$, 0.221 ± 0.002 for $x = 0.9$ while for $x = 1.0$ there are two peaks corresponding to $(0.200 \pm 0.002)c^*$ and $(0.189 \pm 0.002)c^*$. These wavevectors all correspond closely

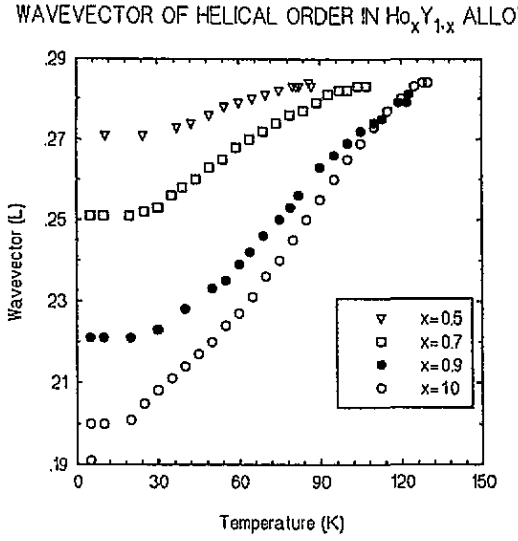

Figure 1. The wavevector of the helical order in Ho_xY_{1-x} alloys as a function of temperature.

to the wavevectors of commensurate structures, $\frac{4}{15}c^*$, $\frac{1}{4}c^*$, $\frac{2}{9}c^*$, $\frac{1}{5}c^*$ and $\frac{4}{21}c^*$, which are consistent with the hexagonal anisotropy and as shown in figure 2 can be labelled by the number of spins close to successive easy axes as (2111), (211), (21), (221) and (2221) structures. These are similar to the structures found theoretically for the ground state of the ANNI model and various clock models. From the relative intensity of the harmonics we have obtained a detailed description of the structures, and the angles of the four principal structures, (221), (21), (211) and (2111), are listed in table 2. The angles determining the structures are θ_1 and θ_2 as defined in figure 2, while the angle between the moments in the blocks of pairs of moments is ψ, and the nearest moment to one of a block of two is φ. Table 2 shows that ψ steadily increases as the wavevector increases, or as the average angle between the spins increases, while φ is close to being constant. The steady behaviour of the trends shown in table 2 gives confidence in the results, and the values for ψ can be compared with those of bulk holmium at low temperatures with $q = \frac{1}{6}c^*$ when $\psi = 11.6°$, and the angle between spins close to different easy axes in 48.4° (Koehler 1972).

Table 1. Parameters of the Ho_xY_{1-x} alloy films.

Nominal concentration	Mosaic spread (deg)	c (lattice parameter) (Å)	x	T_c (K)
1	0.27 ± 0.02	5.6120 ± 0.0010	1	130.7 ± 0.2
0.9	0.18 ± 0.02	5.6261 ± 0.0010	0.88 ± 0.01	123.7 ± 0.2
0.7	0.17 ± 0.02	5.6472 ± 0.0010	0.70 ± 0.01	107.5 ± 0.2
0.5	0.20 ± 0.02	5.6701 ± 0.0010	0.51 ± 0.01	88.4 ± 0.2

4. The phase transition

As discussed in section 1, the behaviour of the phase transition in bulk holmium is still controversial because there are a range of different experimental results and different

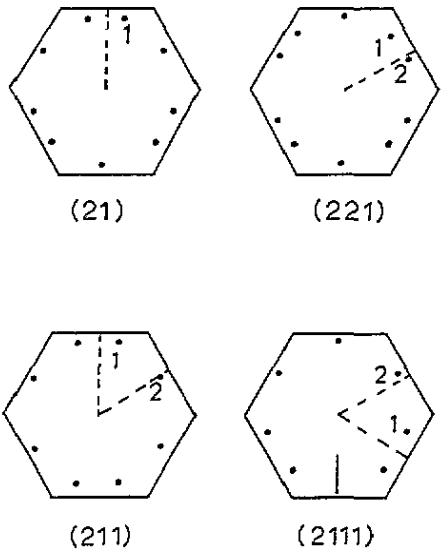

Figure 2. A projection of the moment directions of successive planes for different commensurate structures. The structures are specified by the angles θ between the labelled directions and the nearest easy axes (dotted lines). For the (2111) structure only a (21112) block is shown as the diagram becomes very confusing if a complete projection is shown.

Table 2. Structured parameters of the low-temperature phase of Ho_xY_{1-x}.

Concentration x	Structure	θ_1 (deg)	θ_2 (deg)	ψ (deg)	φ (deg)
1	221	17.0 ± 3	5 ± 3	22 ± 5	43.0 ± 3
0.9	21	13.5 ± 1		27 ± 1	46.5 ± 5
0.7	211	15.5 ± 3	2 ± 3	31 ± 6	46.5 ± 5
0.5	2111	18.0 ± 4	5 ± 2	36 ± 8	47.0 ± 5

theoretical predictions. We decided therefore to measure the behaviour of the magnetic scattering from the holmium and holmium/yttrium films as a function of temperature near to the onset of long-range order, T_c. Most of the experiments were performed by scanning along $(00L)$ with $L \simeq 0.25$, and then fitting the resulting profiles to Gaussian distributions to extract the peak position, width and intensity. Experiments were also performed around $L \simeq 1.75$ and the results for the temperature dependence of the intensity were quantitatively similar. In figure 3, we show the resulting intensities as a function of temperature. Over quite a wide range, the intensity was clearly proportional to $T_c - T$, as shown in figure 3, but close to T_c the intensity was rounded, figure 4, in a way that suggested $\beta > 0.5$. If this rounding arises from critical scattering, then it might be expected that the scattering occurring above T_c would be broader in wavevector than that below. Careful studies, particularly of the transverse width of both the Ho and Ho/Y films, failed to show any broadening or change in wavevector of the scattering in this region. Comparing this result with the x-ray and neutron results obtained by Thurston *et al* (1993) on bulk holmium, it appears that the rounding of the temperature dependence of the intensity may be associated with the second long length scale that they observe, and that the broad critical scattering is too weak to observe from the films. Since our films are capped on both sides by non-

magnetic yttrium, this suggestion would imply that the second length scale may not be associated with the surface. In our films, as in bulk holmium, it could be associated with a change in T_c due to macroscopically large inhomogeneously strained regions. Since our samples are grown epitaxially we expect there to be relatively little change in the strain through the film.

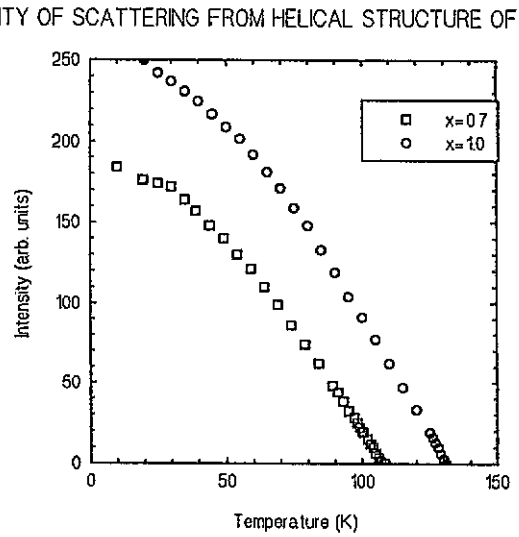

Figure 3. The temperature dependence of the intensity of the magnetic scattering from the Ho film and the $Ho_{0.7}Y_{0.3}$ film.

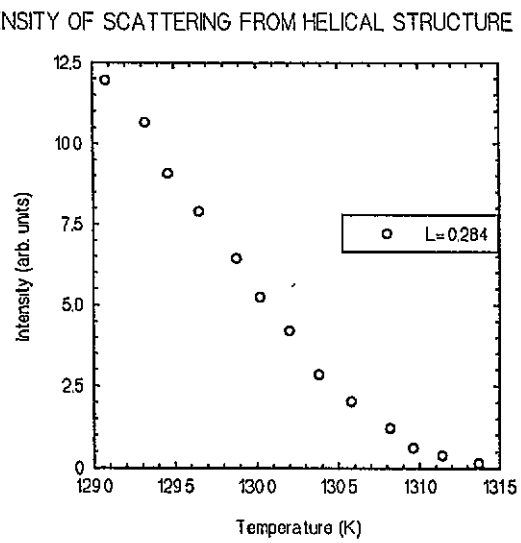

Figure 4. The temperature dependence of the intensity of the magnetic scattering from the Ho film close to T_c.

Table 3. The results of fits to holmium critical scattering data.

Range	T_c (K)	β	σ (K)	χ^2
131.4 → 125	131.05 ± 0.01	0.545 ± 0.028	—	21
130.8 → 125	130.98 ± 0.02	0.527 ± 0.036	—	11
130.4 → 125	130.71 ± 0.02	0.468 ± 0.055	—	2
131.4 → 125	130.60 ± 0.05	0.444 ± 0.085	0.75 ± 0.02	2

Table 4. Fits to holmium/yttrium alloy critical scattering data.

Holmium concentration	Range	T_c (K)	β	σ (K)	χ^2
0.9	123.6 → 120	123.79 ± 0.04	0.549 ± 0.042	—	2
0.9	123.6 → 120	123.67 ± 0.13	0.501 ± 0.084	0.43 ± 0.20	2
0.7	107.1 → 100	107.58 ± 0.03	0.521 ± 0.030	—	3
0.7	108 → 100	107.29 ± 0.04	0.472 ± 0.030	1.02 ± 0.05	1.5
0.5	87 → 76	88.35 ± 0.08	0.542 ± 0.012	—	5

The data were analysed further by fitting the intensities to the conventional exponent relationship

$$I(T) = A(T_c - T)^{2\beta}$$

and allowing the parameters A, T_c and β to vary to get a good fit. The results are listed in table 3 for fits to different temperature ranges to alter the influence of the rounding. We also show a fit to the same function but with a Gaussian spread in T_c with the width specified by a parameter σ. The results shown in table 2 show that the different fits lead to values of β between 0.55 and 0.45 and so it seems reasonable to conclude from the measurements that $\beta = 0.50 \pm 0.05$.

Similar experiments were performed on the alloy samples and similar results were obtained, figure 3, and the results of various fits are listed in table 4. The spread in T_c given by σ is no larger on average than that for bulk holmium, suggesting that the concentration of the alloy films is uniform to better than 0.5%. The values of the exponents derived for the alloys are all, within error, the same as that of the holmium film, namely 0.50±0.05. We conclude therefore that the second length scale is important in both holmium and holmium/yttrium films as well as for bulk holmium, and that within our error there is no difference in the critical properties of holmium and holmium/yttrium alloys, which in turn suggests that the specific heat exponent, α, of bulk holmium is negative.

5. The phase diagram in an applied magnetic field

The alloy sample containing 70% of holmium was mounted in a variable-temperature cryostat, in which the magnetic field was applied perpendicular to the scattering plane. Most of the scans were short scans of the wavevector transfer along $(00L)$ with $L \simeq 0.25$, to identify the different phases that occurred as the temperature and magnetic field were varied and the intensity distributions were fitted to Gaussian profiles. The resulting phase diagram is shown in figure 5. At low fields there is a high-temperature incommensurate helical phase, and a low-temperature commensurate, $L = 0.25$, helical phase as discussed in section 3. On increasing the magnetic field the temperature for the transition to the commensurate phase

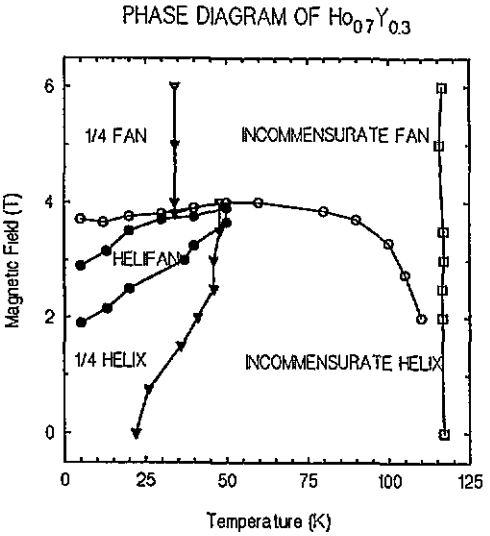

Figure 5. The phase diagram for $Ho_{0.7}Y_{0.3}$ in a magnetic field applied in the basal plane along a hard a-axis. The lines are joining the experimental points for clarity. Above 120 K the system is paramagnetic. The open points give the boundary between the helical and fan phases on increasing the field. On decreasing the field the solid points give the boundary of the helifan phase.

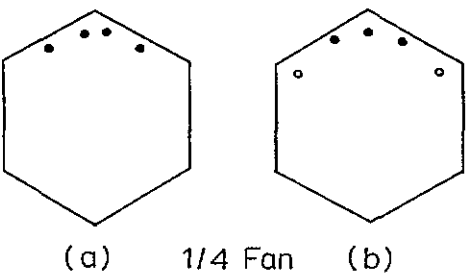

Figure 6. A projection of the structure of the $\frac{1}{4}$ fan phase as deduced from the intensities at 5 K, with the magnetic field applied vertical. In (a) the two angles are $7 \pm 5°$ and $47 \pm 5°$ and the directions shown are present in both senses of the spiral. For structure (b) the angles from the field of successive planes are 0, $25 \pm 5°$, $58 \pm 8°$, $25 \pm 5°$, 0, $-25 \pm 5°$ $-58 \pm 8°$, $-25 \pm 5°$.

increases, showing that the field tends to favour the formation of commensurate phases, as has been found in field-dependent studies of bulk holmium (Cowley *et al* 1991, Jehan *et al* 1992).

At high fields, above 3.8 T, the structure is different, and the results are consistent with a fan phase, as illustrated in figure 6. The evidence for a fan phase comes from a large increase in the scattered intensity at the nuclear Bragg peak (002) showing that there is a basal plane ferromagnetic moment, and a decrease in the intensity of the helical magnetic satellite as shown in figure 7. From these measurements we are able to deduce that the structure of the fan phase is one of the two structures shown in figure 6, and with the parameters as listed in the caption to figure 6. It is unfortunate that the experimental results do not clearly distinguish between these two possible low-temperature structures.

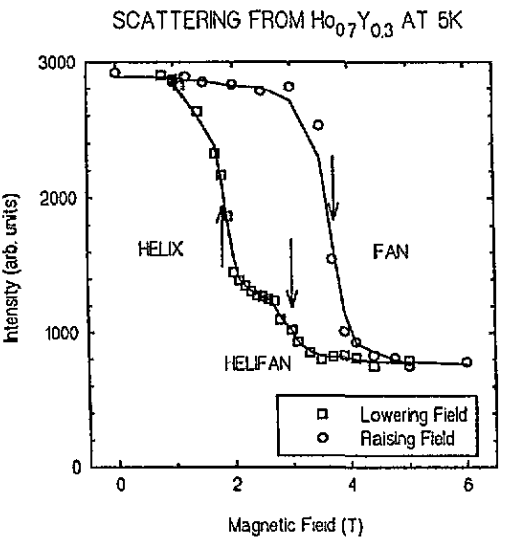

Figure 7. The intensity of the $L = 0.25$ peak in the magnetic scattering of $Ho_{0.7}Y_{0.3}$ at 5 K on increasing and then decreasing the magnetic field. In the former case the structure goes directly from a helical to a fan phase at 3.8 T, but in the latter from a fan to a helifan phase at 3.0 T and then from a helifan to a helical phase at 2.2 T.

The phase boundary between the commensurate and incommensurate fan phase was located from the temperature dependence of the $L = 0.25$ peak, as shown in figures 8 and 9. It was unexpected that there would be a large increase in the intensity of this scattering in the commensurate phase, and it is also to be noted that the temperature dependence near the onset of long-range order, $\sim$ 100 K, is very different from that shown in figure 3. Furthermore the temperature dependence of the wavevector close to the development of the commensurate phase is much sharper in the fan phase, particularly on cooling, than in the helical phase, where there was little difference between heating and cooling, figure 1

Table 5. Intensities and models for the helifan phase at 5 K ($H = 3$ T).

	Intensity				
	$L = 1.5$	$L = 1.67$	$L = 1.75$	$L = 1.83$	$L = 2.00$
Experiment	0.0093	0.061	0.215	0.133	0.156
Model A†	0.0041	0.071	0.250	0.151	0.047
Model B†	0.0069	0.081	0.250	0.137	0.040
Model C†	0.0000	0.077	0.202	0.130	0.146
	Model				
	A	B	C		
θ_1	−67.5	−90	−72		
θ_2	−22.5	−45	−27		
θ_3	22.5	0	0		
θ_4	67.5	45	27		
θ_5	112.5	90	72		
θ_6	157.5	135	117		

† Model A is of the type shown in figure 10a and B and C in figure 10b. The angles to the magnetic field of the moments for the different planes are labelled as described in fig 10.

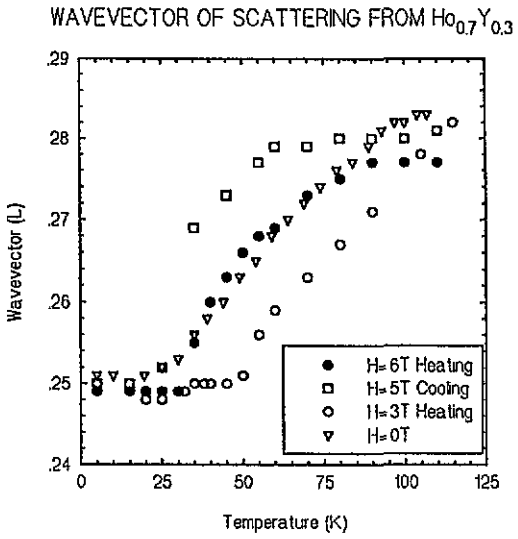

Figure 8. The temperature dependence of the wavevector of the scattering for $Ho_{0.7}Y_{0.3}$ in various applied fields.

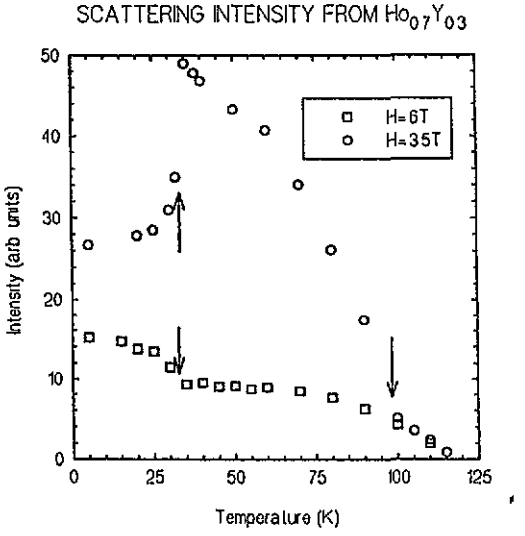

Figure 9. The intensity of the scattering for $L \simeq 0.25$ as a function of increasing temperature for two magnetic fields. At low temperatures with $H = 3.5$ T the structure was a helifan.

The phase boundary between the fan and helical phases was very difficult to locate near the paramagnetic phase. There is some evidence, as shown in part in figure 9, that the boundary decreases to lower fields as the temperature increases. We have not, however, been able to elucidate whether there is a narrow sliver of fan phase persisting down to the critical temperature at $H = 0$.

The phase diagram discussed so far is the phase diagram obtained on raising the magnetic field. The behaviour is different, as shown by figure 7, when the field is reduced. In this

case the fan phase persists to a lower field than that at which the transition from helix to fan occurs, and then forms an intermediate phase, before eventually transforming back to the helical phase at much lower field. The intermediate phase was found to be a helifan phase and magnetic scattering for wavevector transfers along (00L) was observed for $L = 2$, 1.832, 1.750, 1.670, 1.50. There wavevectors are characteristic of the scattering by the simplest helifan structure, described by Jensen and Mackintosh (1990), in which there are 12 moments forming a clockwise helical structure followed by 12 forming an anti-clockwise helix. In figure 10 we show two possible structures for this phase, and in table 5 compare the resulting intensities with the observations. The intensities are normalized by comparison with the scattered intensity with $L = 1.75$ and zero applied field. The first model used was a simple plane-wave helical structure and this gives, not surprisingly, insufficient ferromagnetic scattering at (002), and almost identical intensities for the structures 10(a) and 10(b). Consequently in the next model, all the moments were rotated by a fixed amount towards the magnetic field direction. This gives very reasonable agreement with the experimental results as shown in table 5 for model 10(b), and similarly for a structure based on model 10(a).

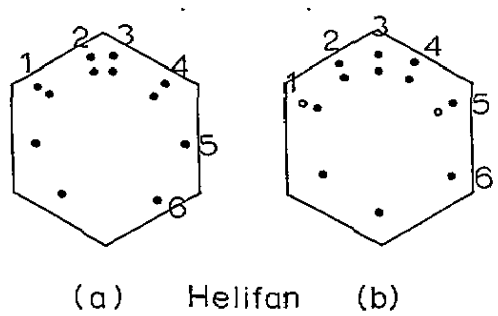

Figure 10. A projection of the moment directions in the clockwise portion of the helifan structure with the magnetic field vertical and with the moments labelled as in table 5. In (a) the anticlockwise helix repeats with the same angles as the clockwise helix while in (b) the open circles show the single planes at the end of the sections common to both helices.

The helifan phase was only obtained by reducing the field from that required for the fan phase. We never observed a transition from the helix to the helifan. Presumably this arises because there is a considerable barrier energy that has to be overcome to create reversals in the sense of the rotation, while forming the helifan from the fan phase is easier because the necessary phase reversals are already present in the fan phase and only some of the phase reversals have to be annihilated.

6. Conclusions

In this paper we have shown that the magnetic structure of random alloys can be studied using the small quantities of the alloys grown by molecular beam epitaxy, MBE. The samples have a mosaic spread of 0.2°, and concentration inhomogeneities of less than 0.5%, and with concentrations within 2% of the nominal values. MBE techniques therefore provide an alternative and in many ways a very convenient way of producing random alloy samples.

Presumably this is because the growth is not under equilibrium conditions and so clustering and concentration gradients are less likely to form.

The magnetic strucutures of the samples were then studied using neutron scattering techniques. Although the samples are only 5000 Å thick there was sufficient intensity for the determination of the magnetic structures. The intensity is, however, too weak for the excitations to be determined. The structures of the four samples of Ho_xY_{1-x}, with $x = 1, 0.9, 0.7$ and 0.5, were determined in zero field. As found initially by Child *et al* (1965) from powder measurements, the structures are ferromagnetic within each basal plane and the Ho^{3+} moments confined to the basal plane. The moments in successive basal planes then rotate to form helical structures described by a wavevector q along the c-axis. At the onset of the long-range order $q = 0.282c^*$, while at low temperature all of the samples form commensurate structures due to the hexagonal anisotropy in the basal planes. The details of these commensurate structures are shown in figure 2. The pure holmium film does not enter the $q = 0.167c^*$ cone phase found in bulk holmium, either because the epitaxial strain alters the interactions, or because the substrate clamps the holmium film thereby inhibiting the transition. Since all of the samples form commensurate structures at low temperatures, it is tempting to argue that the phase diagram as a function of concentration consists of a whole sequence of long-period commensurate phases as predicted by ANNI models or various clock models.

The nature of the phase transition in pure holmium is controversial because neither the theory nor the experiments are yet understood. We have therefore measured the exponent β for all of the films and find that $\beta = 0.50 \pm 0.05$ in each case. The situation is more ambiguous than that implied by this simple statement because the results suggest that there is rounding of T_c by about 0.5° even in the pure holmium film. This rounding is not critical scattering in the normal way, because no broadening in wavevector of the scattering was observed even though quite high resolution was used. This is possibly due to the second long length scale as suggested by Thurston *et al* (1993). Our results were, however, obtained in a sample capped by yttrium and so the surfaces are very different from those of bulk holmium. If our rounding is due to the second length scale, it suggests that the surface properties are not necessarily the controlling feature of whether or not a second length scale exists in holmium, despite the results obtained by Gehring *et al* (1993) on terbium.

The magnetic structure of one sample, $x = 0.7$, was studied when a field was applied in the basal plane. The first result was that the field did not destroy the long-range order. It might have been expected that local fluctuations in the concentration would lead to regions with local ferromagnetic moments that would be aligned by the field. By analogy with the application of a field to a random antiferromagnet to produce a random staggered field, this produces a random field on the helical structure, which would be expected to destroy the long-range order. In contrast we found no evidence for destruction of the order either within the planes or between the planes. Presumably the order within the planes is so strongly formed that this then averages out the effect of the concentration fluctuations.

The magnetic phase diagram was determined in applied magnetic fields as large as 6 T. At high fields > 3.8 T, the structure is a fan phase that is commensurate at low temperature with an eight-plane repeat. The most interesting result was that between the fan phase and the low-field helical phase there was a helifan phase with a 24-plane repeat. This is the only case of a helifan phase observed at low temperature. It is also of interest that the helifan phase can only be formed by reducing the field from the fan phase, and not by increasing the applied field or decreasing the temperature from the helical phases. Further theoretical work is needed to understand the phase diagram in detail.

Acknowledgments

We have benefited from helpful discussions with D Gibbs, D Jehan, D F McMorrow, G Shirane, P Swaddling and T Thurston. RAC is very grateful for the hospitality at Brookhaven. Financial support in Oxford was provided by the Magnetism Initiative of the Science and Engineering Research Council and at Brookhaven by the US DOE under contract No DE-AC 0276 CH 00016.

References

Bak P and Mukamel D 1976 *Phys. Rev.* B **13** 5086
Barak Z and Walker M B 1982 *Phys. Rev.* B **25** 1969
Child H R, Koehler W C, Wollan E O and Cable J W 1965 *Phys. Rev.* A **138** 1655
Cowley R A, Jehan D A, McMorrow D F and McIntyre G J 1991 *Phys. Rev. Lett.* **56** 1521
Eckert J and Shirane G 1976 *Solid State Commun.* **19** 911
Gaulin B D, Hagen M and Child H R 1988 *J. Physique Coll.* **49** C8 327
Gehring P M, Hirota K, Majkrzak C F and Shirane G 1993 *Phys. Rev. Lett.* **71** 1089
Harris A B 1974 *J. Phys. C: Solid State Phys.* **7** 1671
Jayasuruya K D, Campbell S J and Stewart A M 1985 *J. Phys. F: Met. Phys.* **15** 225
Jehan D A, McMorrow D F, Cowley R A and McIntrye G J 1992 *Europhys. Lett.* **17** 553
Jehan D A, McMorrow D F, Cowley R A, Ward R C C, Wells M R, Hagmann N and Clausen K N 1993 *Phys. Rev.* **48** 5594
Jensen J and Mackintosh A R 1990 *Phys. Rev. Lett.* **64** 2699
Kawamura H 1988 *Phys. Rev.* B **38** 4916
Koehler W C 1972 *Magnetic Properties of Rare Earth Metals* ed R J Elliot (London: Plenum) p 81
Kwo J, Gyorgy E M, McWhan D B, Disalvo F J, Vettier C and Bower J E 1985 *Phys. Rev. Lett.* **55** 1402
Thurston T R, Helgesen G, Gibbs D, Hill J P, Gaulin B D and Shirane G 1993 *Phys. Rev. Lett.* **70** 3151
Wang J, Belanger D P and Gaulin B D 1991 *Phys. Rev. Lett.* **66** 3195